Progress In Electromagnetics Research, PIER 60, 221–243, 2006

MODAL ANALYSIS OF A TWO-DIMENSIONAL DIELECTRIC GRATING SLAB EXCITED BY AN OBLIQUELY INCIDENT PLANE WAVE

A. M. Attiya

Electronics Research Institute
El-Tahreer St., Dokki, Gizza, Egypt

A. A. Kishk

Department of Electrical Engineering
and Center for Electromagnetic System Research (CESR)
University of Mississippi
University, MS 38677, USA

Abstract—A vectorial modal analysis of two-dimensional (2-D) dielectric grating is presented. The transmission and reflection from the 2-D dielectric-grating slab are computed by combining the generalized scattering matrix and the modal analysis. New insights on the boundary conditions between two grating structures are presented to be suitable for two-dimensional gratings. The results obtained using the present analysis are verified with published experimental and numerical results for both one- and two-dimensional dielectric-grating slabs. The present approach provides fast convergence and provides good agreement with other numerical techniques. This technique is used to study the effects of different parameters for designing a wide band FSS composed of multilayered 2-D grating slabs.

1. INTRODUCTION

Due to the filtering and diffractive effects of their periodic structures, dielectric gratings have found different applications in controlling the propagation of electromagnetic waves. They can be used as frequency-selective surfaces. They can also be used as substrates or superstrates for microstrip antennas to suppress the excitation of surfaces waves or be used in microstrip circuits to add filtering effects on simple guiding structures like microstrip lines. These applications and others were the

motivation to introduce comprehensive studies of different dielectric grating structures using different techniques during last two decades [1–12]. These techniques can be classified into two main categories, numerical techniques such as method of moment [7] and finite difference time domain [9] and semi-analytical techniques such as transverse resonance technique [3–5, 10] and modal analysis [1, 2, 11, 12]. The main advantage of numerical techniques is that they can easily include any perturbation in finite periodic structure as well as solving infinite periodic structures. On the other hand, semi-analytical techniques are mainly valid for infinite periodic structures. However, these techniques require much less computational effort to obtain the characteristics of the grating structure. Vectorial modal analysis showed important advantage compared with transverse resonance approach for modeling one-dimensional grating structure where the complexity of the former does not increase with the number of dielectric slabs present in the unit cell as it is usually happens in the latter approach [1]. Another important advantage of vectorial modal analysis compared with the transverse resonance method is that it can be extended to two-dimensional structure as it is used for solving a waveguide filled with inhomogeneous materials [13]. In vectorial modal analysis, the presence of losses in dielectric slabs can be easily considered by simply introducing complex permittivity [1].

It can be expected that by using semi-analytical techniques to obtain the reflection and transmission coefficients of grating structures, it may be possible to formulate Greens function of a point source above grating structure. This formulation can be quite useful for simulating an antenna above grating structure by using integral equation approach. Therefore, the present work extends the vectorial modal analysis of one-dimensional dielectric grating to the case of two-dimensional dielectric grating.

Figure 1 shows a schematic diagram of the proposed problem for a simple case of a single layer-grating slab. It should be noted that for the case of one dimensional grating, where the embedded dielectrics are rectangular rods of finite width along the periodic direction and equal to the dielectric thickness, h. The problem of two-dimensional dielectric grating layered structure can be presented as a multi-section guiding structure of finite thicknesses and infinite lateral dimensions. Each guiding structure consists of periodic dielectric rods embedded in a base dielectric periodic cell. The fields inside each guiding structure are determined in terms of its modes. Thus, the vectorial modal analysis of dielectric grating slabs starts with finding the modes of each layer. Then the boundary conditions are obtained by matching the tangential fields on the interface between the different layers.

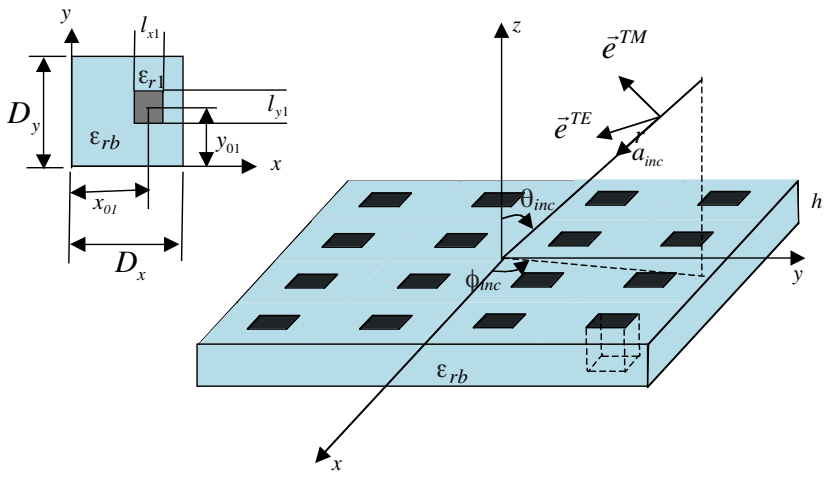

Figure 1. Two-dimensional dielectric grating slab excited by obliquely incident plane wave.

By enforcing obtaining the appropriate boundary conditions, one can obtain the reflection and transmission coefficients from one grating structure to the other. Then by using the generalized scattering matrix approach one can obtain the transmission and reflection of multilayered grating structure [14]. The details of the modal analysis for two-dimensional dielectric grating structures are discussed in Section 2. Then the problems of the boundary conditions and the generalized scattering matrix are discussed in Section 3. Sample results and discussions are presented in Section 4.

2. MODAL ANALYSIS OF TWO-DIMENSIONAL DIELECTRIC GRATING

Starting from Maxwell's equations, it can be shown that for spatial dependent medium the wave equation of the magnetic field is

$$\nabla \times \left(\varepsilon_r^{-1} \nabla \times \vec{H}\right) = k_0^2 \vec{H} \tag{1}$$

For the case of a guiding structure, ε_r is independent of its longitudinal direction and the field dependence on the longitudinal direction is $e^{-j\beta z}$, assuming that z is the longitudinal direction. Thus, the transverse field part of (1) can be rewritten as follows:

$$\left[\nabla_t^2 + k_0^2 \varepsilon_r + \left(\frac{\nabla_t \varepsilon_r}{\varepsilon_r}\right) \times (\nabla_t \times \circ)\right] \vec{h}_t = \beta^2 \vec{h}_t \tag{2}$$

where $\vec{h}_t$ is the field distribution of the transverse magnetic field components. By solving this eigen value problem, one can obtain the field distribution of the transverse magnetic field $\vec{h}_t$ and the propagation constant β. The solution requires expanding the transverse magnetic field in terms of a set of orthogonal Floquet mode expansion functions. These expansions are obtained for the TE and TM modes separately, which requires use of bi-orthogonal functions to represent each mode separately.

It is important to choose such bi-orthogonal expansion functions. In previous studies of one-dimensional dielectric grating, the plane consisting of the direction of incidence and the normal direction to the interface between the dielectric layers of the same grating structure is considered as the plane of incidence. Then, the TE and TM directions are defined based on this plane. Such definition simplifies the relation between the transverse magnetic field obtained by solving the above eigen value problem and the transverse electric field [1, 4]. However, this approach cannot be applied for two-dimensional grating because there is no fixed normal direction to the interface between the embedded dielectric rods and the surrounding dielectric base medium. Thus, it would be preferred to define the plane of incidence as the plane consisting of the direction parallel to the embedded rods, which is the z direction, and the direction of incidence. The advantage of this choice is that it would be consistent with the traditional definition of the TE and TM wave for planar structure. For arbitrary incident plane wave, the direction of incidence is

$$\vec{a}_{\text{inc}} = \sin\theta_{\text{inc}}\cos\phi_{\text{inc}}\vec{a}_x + \sin\theta_{\text{inc}}\sin\phi_{\text{inc}}\vec{a}_y - \cos\theta_{\text{inc}}\vec{a}_z \tag{3}$$

Thus, the unit vectors of the TE and TM transverse magnetic fields are

$$\vec{a}_{hTE} = \cos\phi_{\text{inc}}\vec{a}_x + \sin\phi_{\text{inc}}\vec{a}_y \tag{4a}$$

$$\vec{a}_{hTM} = -\sin\phi_{\text{inc}}\vec{a}_x + \cos\phi_{\text{inc}}\vec{a}_y \tag{4b}$$

Based on the above definition of TE and TM magnetic field directions, it can be assumed that the bi-orthogonal Floquet mode expansion functions can be defined as

$$\vec{\tilde{h}}^{TE}_{mn} = \frac{\exp(-jk_{xm}x - jk_{yn}y)}{\sqrt{D_xD_y}}(\cos\phi_{\text{inc}}\vec{a}_x + \sin\phi_{\text{inc}}\vec{a}_y) \tag{5a}$$

$$\vec{\tilde{h}}^{TM}_{mn} = \frac{\exp(-jk_{xm}x - jk_{yn}y)}{\sqrt{D_xD_y}}(-\sin\phi_{\text{inc}}\vec{a}_x + \cos\phi_{\text{inc}}\vec{a}_y) \tag{5b}$$

where

$$k_{xm} = k_{x0} + 2\pi m/D_x \tag{5c}$$

$$k_{yn} = k_{y0} + 2\pi n/D_y \tag{5d}$$
$$k_{x0} = k_0 \sin\theta_{\text{inc}} \cos\phi_{\text{inc}} \tag{5e}$$
$$k_{y0} = k_0 \sin\theta_{\text{inc}} \sin\phi_{\text{inc}} \tag{5f}$$

D_x and D_y are the dimensions of the periodic cell. The bi-orthogonality relation can be easily verified as follows

$$\left\langle \vec{\tilde{h}}^{\zeta}_{mn}, \vec{\tilde{h}}^{\xi}_{m'n'} \right\rangle = \int_0^{D_x}\int_0^{D_y} \vec{\tilde{h}}^{\zeta^*}_{mn} \cdot \vec{\tilde{h}}^{\xi}_{m'n'} dxdy = \delta_{mm'}\delta_{nn'}\delta_{\zeta\xi} \tag{6}$$

Using these bi-orthogonal expansion functions, the transverse magnetic field component can be represented as

$$\vec{h}_t = \vec{h}_t^{TE} + \vec{h}_t^{TM} = \sum_p C^{TE}_{(p)} \vec{\tilde{h}}^{TE}_{(p)} + C^{TM}_{(p)} \vec{\tilde{h}}^{TM}_{(p)} \tag{7}$$

where each (p) represents different combinations of mn. Ideally, this series should be infinite. However, for numerical implementation this series is truncated to be finite. The problem of obtaining the transverse magnetic field distribution is now converted into obtaining the amplitudes of such modal expansion. By inserting (7) into (12), one can obtain

$$L\vec{h}_t = \sum_p C^{TE}_{(p)} L\vec{\tilde{h}}^{TE}_{(p)} + C^{TM}_{(p)} L\vec{\tilde{h}}^{TM}_{(p)} = \beta^2 \sum_p C^{TE}_{(p)} \vec{\tilde{h}}^{TE}_{(p)} + C^{TM}_{(p)} \vec{\tilde{h}}^{TM}_{(p)} \tag{8a}$$

where

$$L = L_0 + \Delta_1 + \Delta_2 \tag{8b}$$
$$L_0 = \nabla_t^2 + k_0^2 \varepsilon_{rb} \tag{8c}$$
$$\Delta_1 = k_0^2 \left(\varepsilon_r(x,y) - \varepsilon_{rb}\right) \tag{8d}$$
$$\Delta_2 = \left(\frac{\nabla_t \varepsilon_r(x,y)}{\varepsilon_r(x,y)}\right) \times (\nabla_t \times \circ) \tag{8e}$$

To obtain the unknown amplitudes of the field expansion functions and the corresponding propagation constant of each mode convert (8a) into an eigen value problem as follows

$$\begin{bmatrix} \left[L^{TE/TE}_{pq}\right] & \left[L^{TE/TM}_{pq}\right] \\ \left[L^{TM/TE}_{pq}\right] & \left[L^{TM/TM}_{pq}\right] \end{bmatrix} \begin{bmatrix} \left[C^{TE}_{(q)}\right] \\ \left[C^{TM}_{(q)}\right] \end{bmatrix} = \beta^2 \begin{bmatrix} \left[C^{TE}_{(q)}\right] \\ \left[C^{TM}_{(q)}\right] \end{bmatrix} \tag{9a}$$

where

$$L_{pq}^{TE/TE} = \left\langle \vec{\tilde{h}}_{(p)}^{TE}, L_0 \vec{\tilde{h}}_{(q)}^{TE} \right\rangle + \left\langle \vec{\tilde{h}}_{(p)}^{TE}, \Delta_1 \vec{\tilde{h}}_{(q)}^{TE} \right\rangle + \left\langle \vec{\tilde{h}}_{(p)}^{TE}, \Delta_2 \vec{\tilde{h}}_{(q)}^{TE} \right\rangle \quad (9b)$$

$$L_{pq}^{TE/TM} = \left\langle \vec{\tilde{h}}_{(p)}^{TE}, \Delta_2 \vec{\tilde{h}}_{(q)}^{TM} \right\rangle \quad (9c)$$

$$L_{pq}^{TM/TE} = \left\langle \vec{\tilde{h}}_{(p)}^{TM}, \Delta_2 \vec{\tilde{h}}_{(q)}^{TE} \right\rangle \quad (9d)$$

$$L_{pq}^{TM/TM} = \left\langle \vec{\tilde{h}}_{(p)}^{TM}, L_0 \vec{\tilde{h}}_{(q)}^{TM} \right\rangle + \left\langle \vec{\tilde{h}}_{(p)}^{TM}, \Delta_1 \vec{\tilde{h}}_{(q)}^{TM} \right\rangle + \left\langle \vec{\tilde{h}}_{(p)}^{TM}, \Delta_2 \vec{\tilde{h}}_{(q)}^{TM} \right\rangle \quad (9e)$$

It should be noted that the operator Δ_2 is the only part of the operator L that can couple TE and TM waves. By obtaining the eigen values and the eigen vectors of (9), one can obtain the field distribution of each mode by using (7) and its corresponding propagation factor.

For the case of a grating consisting of rectangular dielectric rods, the relative dielectric constant at each cell can be represented as

$$\begin{aligned} \varepsilon_r(x,y) = \varepsilon_{rb} + \sum_{i=1}^{ND} [(\varepsilon_{ri} - \varepsilon_{rb})(H(x - x_{0i} + l_{xi}/2) - H(x - x_{0i} - l_{xi}/2)) \\ \times (H(y - y_{0i} + l_{yi}/2) - H(y - y_{0i} - l_{yi}/2))] \end{aligned} \quad (10)$$

where $H(\,)$ is the Heaviside unit step function, (x_{0i}, y_{0i}) is the center of the i^{th} rod, l_{xi} and l_{yi} and are the dimensions, and ND is the number of dielectric rods in unit cell. Using (8) and (10) into (9) a closed form for the matrix elements in (9) as

$$\begin{aligned} L_{pq}^{TE/TE} = {} & \tilde{\beta}_p^2 \delta_{pq} + k_0^2 R_0 \left(k_{x(p)} - k_{x(q)}, k_{y(p)} - k_{y(q)} \right) \\ & + \left(j k_{x(q)} \sin\phi_{\text{inc}} - j k_{y(q)} \cos\phi_{\text{inc}} \right) \\ & \times \left(R_{1y} \left(k_{x(p)} - k_{x(q)}, k_{y(p)} - k_{y(q)} \right) \cos\phi_{\text{inc}} \right. \\ & \left. - R_{1x} \left(k_{x(p)} - k_{x(q)}, k_{y(p)} - k_{y(q)} \right) \sin\phi_{\text{inc}} \right) \end{aligned} \quad (11a)$$

$$\begin{aligned} L_{pq}^{TM/TM} = {} & \tilde{\beta}_p^2 \delta_{pq} + k_0^2 R_0 \left(k_{x(p)} - k_{x(q)}, k_{y(p)} - k_{y(q)} \right) \\ & + \left(j k_{x(q)} \cos\phi_{\text{inc}} + j k_{y(q)} \sin\phi_{\text{inc}} \right) \\ & \times \left(-R_{1y} \left(k_{x(p)} - k_{x(q)}, k_{y(p)} - k_{y(q)} \right) \sin\phi_{\text{inc}} \right. \\ & \left. - R_{1x} \left(k_{x(p)} - k_{x(q)}, k_{y(p)} - k_{y(q)} \right) \cos\phi_{\text{inc}} \right) \end{aligned} \quad (11b)$$

$$
\begin{aligned}
L_{pq}^{TE/TM} &= \left(jk_{x(q)}\cos\phi_{\text{inc}} + jk_{y(q)}\sin\phi_{\text{inc}}\right) \\
&\quad \times \left(R_{1y}\left(k_{x(p)}-k_{x(q)}, k_{y(p)}-k_{y(q)}\right)\cos\phi_{\text{inc}}\right. \\
&\quad \left. -R_{1x}\left(k_{x(p)}-k_{x(q)}, k_{y(p)}-k_{y(q)}\right)\sin\phi_{\text{inc}}\right) \qquad (11c) \\
L_{pq}^{TM/TE} &= \left(jk_{x(q)}\sin\phi_{\text{inc}} - jk_{y(q)}\cos\phi_{\text{inc}}\right) \\
&\quad \times \left(-R_{1y}\left(k_{x(p)}-k_{x(q)}, k_{y(p)}-k_{y(q)}\right)\sin\phi_{\text{inc}}\right. \\
&\quad \left. -R_{1x}\left(k_{x(p)}-k_{x(q)}, k_{y(p)}-k_{y(q)}\right)\cos\phi_{\text{inc}}\right) \qquad (11d)
\end{aligned}
$$

where

$$
\begin{aligned}
\tilde{\beta}_p &= \sqrt{\varepsilon_{rb}k_0^2 - k_{x(p)}^2 - k_{y(p)}^2} \qquad (12a) \\
R_0(k_x,k_y) &= \frac{1}{D_xD_y}\sum_{i=1}^{ND} 4(\varepsilon_{ri}-\varepsilon_{rb}) \\
&\quad \frac{\sin(k_xl_{xi}/2)}{k_x}\frac{\sin(k_yl_{yi}/2)}{k_y}e^{j(k_xx_{0i}+k_yy_{0i})} \qquad (12b) \\
R_{1x}(k_x,k_y) &= \frac{1}{D_xD_y}\sum_{i=1}^{ND} 8j\frac{(\varepsilon_{ri}-\varepsilon_{rb})}{(\varepsilon_{ri}+\varepsilon_{rb})} \\
&\quad \sin(k_xl_{xi}/2)\frac{\sin(k_yl_{yi}/2)}{k_y}e^{j(k_xx_{0i}+k_yy_{0i})} \qquad (12c) \\
R_{1y}(k_x,k_y) &= \frac{1}{D_xD_y}\sum_{i=1}^{ND} 8j\frac{(\varepsilon_{ri}-\varepsilon_{rb})}{(\varepsilon_{ri}+\varepsilon_{rb})} \\
&\quad \frac{\sin(k_xl_{xi}/2)}{k_x}\sin(k_yl_{yi}/2)e^{j(k_xx_{0i}+k_yy_{0i})} \qquad (12d)
\end{aligned}
$$

Up to this point one can obtain the distribution of the transverse magnetic field of each mode and its propagation constant.

3. BOUNDARY CONDITIONS ON THE INTERFACE BETWEEN TWO ADJACENT DIELECTRIC GRATINGS

The tangential magnetic and electric fields should be continuous on the interface between adjacent dielectric gratings. The continuity of the tangential magnetic field can be obtained directly by using the modal representation obtained in the previous section as follows:

$$(I - R_{11})C_1 = T_{21}C_2 \qquad (13)$$

where R_{11} is the reflection matrix at the first grating structure, T_{21} is the transmission matrix from the first grating to the second grating, C_1 and C_2 are the transpose matrix consisting of the eigen vectors corresponding to the modal analyses of the first and the second grating, respectively.

The problem now is to obtain the tangential electric field. It should be noted that the transverse electric field distribution could be obtained via another eigen value problem similar to (1) of the transverse magnetic field [1]. However, obtaining the electric field distribution only is not sufficient to obtain the second boundary condition because it does not present the relation between the amplitude of the transverse electric field and the transverse magnetic field for each mode, which is also required to obtain the second boundary condition. Thus, it is required to obtain the transverse electric field in terms of the obtained transverse magnetic field. For the case of one-dimensional grating, this problem is simplified by appropriate choice of TE and TM definitions as mentioned in the previous section. In this case, the relation between the transverse electric and magnetic fields are only multiplication factors, which represent the TE and the TM characteristic impedances [1, 4]. In this case the TE characteristic impedance is independent of the variation of the dielectric constant. However, in the present case the relation between the transverse electric and magnetic fields cannot be just multiplication factors. To find this relation, it would be required to obtain the transverse electric field in terms of the total magnetic field including the longitudinal magnetic field component. The longitudinal magnetic field component in terms of the transverse magnetic components can be obtained as

$$h_z = -j\beta^{-1}\left(\nabla_t \cdot \vec{h}_t\right) \tag{14}$$

Thus the transverse electric field can be obtained in terms of the transverse magnetic field as follows:

$$j\omega\varepsilon_0\varepsilon_r\vec{e}_t = \left[\nabla_t \times \vec{a}_z\left(-j\beta^{-1}\nabla_t \cdot \vec{h}_t\right) - j\beta\vec{a}_z \times \vec{h}_t\right] \tag{15}$$

Using the modal representation of the transverse magnetic field, (15) can be rewritten in a modal form as:

$$j\omega\varepsilon_0\varepsilon_r\vec{e}_t = \left[\left(-j\beta^{-1}C\left(\nabla_t \times \vec{a}_z\right)\nabla_t \cdot \vec{\tilde{h}}_t\right) - j\beta C\vec{a}_z \times \vec{\tilde{h}}_t\right]$$

where $\vec{\tilde{h}}_t$ is a vector including the TE and TM expansion modes $\vec{\tilde{h}}_t = \left[\left[\vec{\tilde{h}}^{TE}_{(p)}\right]\ \left[\vec{\tilde{h}}^{TM}_{(p)}\right]\right]^T$, β is a diagonal matrix including the propagation

constants of the different modes and C is the transpose matrix consisting of the eigen vectors of the modal analysis for the transverse magnetic field. Assuming that the transverse electric field is expanded in terms of transverse modal functions corresponding to TE and TM modes $\vec{\tilde{e}}_t = \left[\left[\vec{\tilde{e}}^{TE}_{(p)}\right] \ \left[\vec{\tilde{e}}^{TE}_{(p)}\right]\right]^T$ as

$$\vec{e}_t = \vec{e}_t^{TE} + \vec{e}_t^{TM} = \sum_p \Phi^{TE}_{(p)} \vec{\tilde{e}}^{TE}_{(p)} + \Phi^{TM}_{(p)} \vec{\tilde{e}}^{TM}_{(p)} \tag{16}$$

where $\vec{\tilde{e}}^{TE}_{(p)} = -\vec{a}_z \times \vec{\tilde{h}}^{TE}_{(p)}$ and $\vec{\tilde{e}}^{TM}_{(p)} = -\vec{a}_z \times \vec{\tilde{h}}^{TM}_{(p)}$. The electric field amplitude matrix Φ can be obtained by using the bi-orthogonal property of the electric field modal expansion function as follows:

$$j\omega\varepsilon_0 \left\langle \vec{\tilde{e}}, \varepsilon_r \vec{e}_t \right\rangle = \left\langle \vec{\tilde{e}}, \left[\left(-j\beta^{-1} C(\nabla_t \times \vec{a}_z)\nabla_t \cdot \vec{\tilde{h}}_t \right) - j\beta C \vec{a}_z \times \vec{\tilde{h}}_t \right] \right\rangle \tag{17}$$

By solving (17), it can be shown that the electric field amplitude matrix Φ is

$$\Phi = \frac{1}{j\omega\varepsilon_0} \left(-j\beta^{-1} CAA^T + j\beta C \right) \Psi^{-1} \tag{18}$$

where $A = \begin{bmatrix} A^{TE} \\ A^{TM} \end{bmatrix}$ and $\Psi = \begin{bmatrix} \Psi^{TE} & 0 \\ 0 & \Psi^{TM} \end{bmatrix}$. A^{TE} is a diagonal matrix whose element is $(-jk_{x(p)} \cos\phi_{\text{inc}} - jk_{y(p)} \sin\phi_{\text{inc}})$ and A^{TM} is a diagonal matrix whose element is $(jk_{x(p)} \sin\phi_{\text{inc}} - jk_{y(p)} \cos\phi_{\text{inc}}) \cdot$ $\Psi^{TE} = \Psi^{TM}$ is a matrix with element given as

$$\psi_{pq} = \frac{1}{D_x D_y} \int_0^{D_x} \int_0^{D_y} \varepsilon_r(x,y) e^{j(k_{x(p)} - k_{x(q)})x} e^{j(k_{y(p)} - k_{y(q)})y} dxdy$$

After obtaining the transverse electric field amplitude matrix in terms of the previously obtained transverse magnetic field amplitude matrix, one can obtain the equation of the second boundary condition as:

$$(I + R_{11})\Phi_1 = T_{21}\Phi_2 \tag{19}$$

Solving (13) and (19) simultaneously, one can obtain the reflection and transmission matrices as:

$$T_{21} = 2\left(C_2 C_1^{-1} + \Phi_2 \Phi_1^{-1} \right)^{-1} \tag{20a}$$

$$R_{11} = I - 2\left(C_2 C_1^{-1} + \Phi_2 \Phi_1^{-1} \right)^{-1} C_2 C_1^{-1} \tag{20b}$$

The reflection at the second grating structure and the transmission can be obtained from the second to the first grating by exchanging the subscripts 1 and 2 in (20).

In practices, two homogeneous media at both sides of the layered structure surround the layered grating slabs. However, to facilitate the analysis it is assumed that such homogeneous media are composed of grating structure of the same cell size of the slab gratings. The base dielectric constants of these two semi-infinite gratings are the dielectric constants of the two surrounding media and there are no embedded rods in such media. For such homogenous medium the C matrix is simply a unit matrix, $\beta = \begin{bmatrix} \beta^{TE} & 0 \\ 0 & \beta^{TM} \end{bmatrix}$ where $\beta^{TE} = \beta^{TM}$ are diagonal matrices whose elements are $\sqrt{\varepsilon_r k_0^2 - k_{x(p)}^2 - k_{y(p)}^2}$.

The above analysis is suitable to obtain the reflection and transmission matrices between two semi-infinite grating structures. This analysis can be combined with generalized scattering matrix approach to obtain the reflection and transmission from a multilayered medium composed of grating slabs. It should be noted that the word "layer" here means a grating slab and should not be confused with the structure of the grating itself. As a special case, one can obtain the reflection and transmission matrices of a grating slab in free space as follows:

$$\tilde{R}_{11} = R_{11} + T_{12}\left(I - BR_{22}BR_{22}\right)^{-1} BR_{22}BT_{21} \quad (21a)$$

$$\tilde{T}_{12} = T_{12}\left(I - BR_{22}BR_{22}\right)^{-1} BT_{21} \quad (21b)$$

where medium 1 is assumed to be free space and medium 2 is the grating slab, B is a diagonal matrix whose element is $\exp(-j\beta_i h)$, β_i is the ith modal propagation constant of the grating structure, and h is the thickness of the grating slab.

4. RESULTS AND DISCUSSIONS

In this section, different examples are presented to show the validity of the above formulation. These examples include both one- and two-dimensional grating structures. It should be noted that one-dimensional grating can be treated as a two-dimensional grating whose embedded rods extend in one direction up to the cell boundaries. For the sake of comparison with previously mentioned results, it should be noted that the TE case corresponds to electric field normal to the plane of incidence and parallel to the interface between the grating layers and TM case corresponds to electric field parallel to the plane incidence normal to that direction, which is consistent with the present

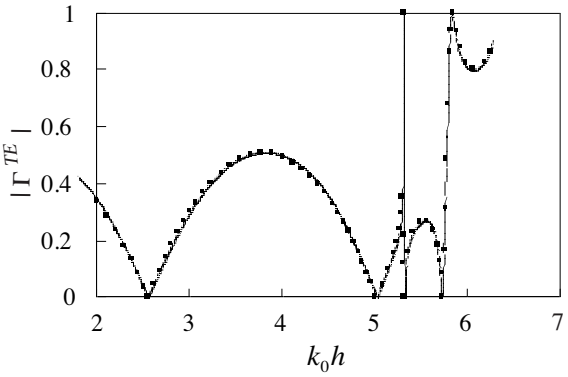

Figure 2. Comparison between Transverse Resonance Method [5] (Dotted points) and Vectorial modal analysis (Solid line) for calculating TE reflection coefficient of a one-dimensional grating with $\varepsilon_{rb} = 1.44$, $\varepsilon_{r1} = 2.56$, $D_x = D_y = 10\,\text{mm}$, $l_{x1} = 10\,\text{mm}$, $l_{y1} = 5\,\text{mm}$, $x_{01} = 5\,\text{mm}$, $y_{01} = 7.5\,\text{mm}$ and $h = 17.13\,\text{mm}$. $\phi_{\text{inc}} = 90^\circ$ and $\theta_{\text{inc}} = 45^\circ$.

definition of TE and TM if it is assumed that the direction parallel to the interface between the layers of the one-dimensional gratings is the x-direction and ϕ_{inc} is $\pi/2$. Other choices are also possible.

Figure 2 shows the TE reflection of a one-dimensional dielectric-grating slab whose base dielectric constant $\varepsilon_{rb} = 1.44$. It includes only one dielectric rod per cell. The dielectric constant of such dielectric rod is $\varepsilon_{r1} = 2.56$. The unit cell is a square of length 10 mm. The dimension of the embedded dielectric rod is 10 mm $\times$ 5 mm. The thickness of the substrate is 17.13 mm. The direction of the incident plane wave is $\phi_{\text{inc}} = \pi/2$ and $\theta_{\text{inc}} = \pi/4$. Excellent agreement is obtained between the present results and the previously published result of Bertoni *et al.* [5, Fig. 3], which is obtained by using transverse resonance method.

Figure 3 presents another example of a one-dimensional dielectric-grating slab, where it presents the transmission coefficients for both TE and TM incident waves. The base dielectric is free space and the dielectric constant of the embedded rods is $\varepsilon_{r1} = 2.59$. The loss tangent of the dielectric rods is $\tan\delta = 0.0067$. The unit cell is a square of length 30 mm. The dimension of the embedded dielectric rod is 30 mm $\times$ 15 mm. The thickness of the substrate is 8.7 mm. The direction of the incident plane wave is $\phi_{\text{inc}} = \pi/2$ and $\theta_{\text{inc}} = \pi/180$. These results show good agreements when compared with the corresponding experimental results of Tibuleac *et al.* [8]. It should be noted that all these results have been obtained by using only

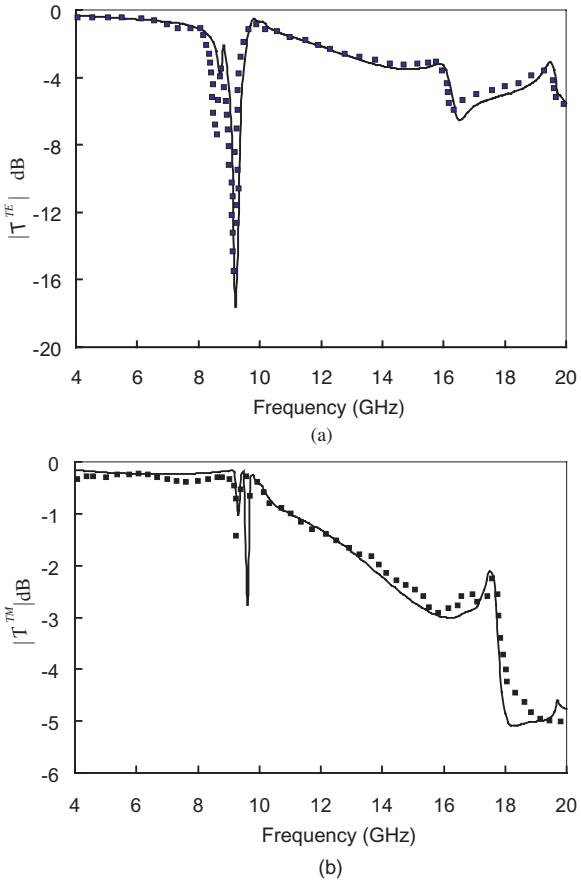

Figure 3. Comparisons between measured [8] and calculated TE and TM transmission coefficients of a one-dimensional grating with $\varepsilon_{rb} = 1$, $\varepsilon_{r1} = 2.59$, $\tan\delta_1 = 0.0067$, $D_x = D_y = 30\,\text{mm}$, $l_{x1} = 30\,\text{mm}$, $l_{y1} = 15\,\text{mm}$, $x_{01} = 15\,\text{mm}$, $y_{01} = 22.5\,\text{mm}$ and $h = 8.7\,\text{mm}$. $\phi_{\text{inc}} = 90^\circ$ and $\theta_{\text{inc}} = 1^\circ$. Measurements are dotted points and calculated results are solid lines. (a) TE, (b) TM.

25 Floquet mode expansion functions where $-2 \leq m, n \leq 2$ in (5).

Figure 4 presents an example of the TM reflection of a two-dimensional dielectric grating slab. The base dielectric is $\varepsilon_{rb} = 4$ and the dielectric constant of the embedded rods is $\varepsilon_{r1} = 10$. The unit cell is a square of length 20 mm and the cross section of the embedded rod is also square of length 10 mm. The thickness of the substrate is 2 mm. The ϕ_{inc} angle is fixed to be zero degree while θ_{inc}

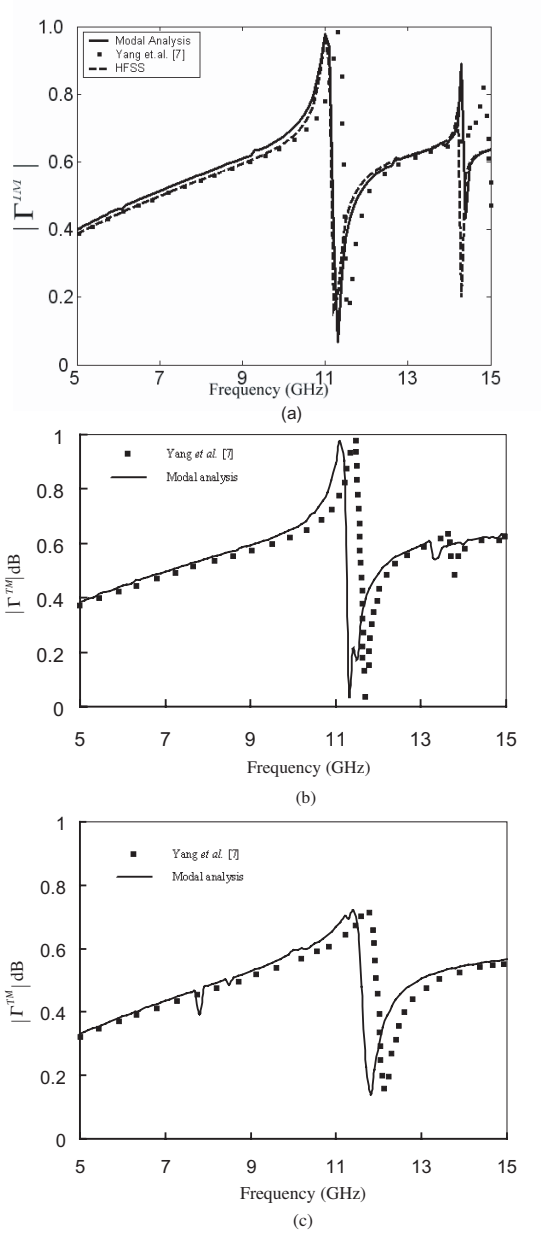

Figure 4. TM reflection coefficients of a two-dimensional grating with $\varepsilon_{rb} = 4$, $\varepsilon_{r1} = 10$, $D_x = D_y = 20\,\text{mm}$, $l_{x1} = 10\,\text{mm}$, $l_{y1} = 10\,\text{mm}$, $x_{01} = 10\,\text{mm}$, $y_{01} = 10\,\text{mm}$ and $h = 2\,\text{mm}$. $\phi_{\text{inc}} = 0^\circ$ and (a) $\theta_{\text{inc}} = 0^\circ$, (b) $\theta_{\text{inc}} = 15^\circ$ and (c) $\theta_{\text{inc}} = 30^\circ$.

has three values namely, 0, 15 and 30 degrees. These results show good agreement with the corresponding results obtained by Method of Moment solution of Yang *et al.* [7]. However, it is noted that there is a fixed difference in the resonance frequency between their results and the present results. This is examined by increasing the number of the Floquet mode expansion functions. It is found that the present solution is highly convergent. Thereforethe same problem is simulated by HFSS for the case of normal incidence. The three results are compared in Fig. 4(a). It can be noted that there is an excellent agreement between the results of HFSS simulation and the results of the vectorial modal analysis. The main advantage of the present technique is the fast convergence as compared with the Method of Moment solution where the present results are obtained by using only 49 Floquet mode expansion functions, $-3 \leq m,\ n \leq 3$, where each mode represent an expansion function whereas Yang *et al.* [7] used 1681 Floquet modes combined with 9 expansion functions to obtain his results.

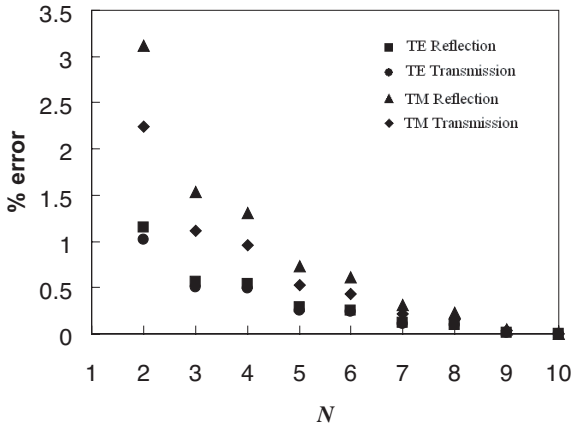

Figure 5. Percentage error of TE and TM transmission and reflection coefficients as functions of the number of Floquet mode expansion functions $-N \leq m, n \leq N$. The percentage error is compared with the results of $m = n = 10$. The grating structure is the same as shown in Fig. 4. $\theta_{\text{inc}} = 30^\circ$ and $\phi_{\text{inc}} = 0^\circ$, $f = 10\,\text{GHz}$.

To show the fast convergence of the present technique, Fig. 5 shows the percentage error of TE and TM transmission and reflection coefficients as a function of the number of Floquet mode expansion functions. The grating structure is the same as that of Fig. 4. The angle of incidence is $\theta_{\text{inc}} = 30^\circ$ and $\phi_{\text{inc}} = 0^\circ$, and the operating frequency is 10 GHz. The Floquet mode expansion functions are

determined as $-N \leq m,\ n \leq N$. The errors are computed based on the solutions obtained with $N = 10$ to be the exact one. It can be noted that, for $N = 2$ the maximum percentage error is less than 4%. The error decreases monotonically as N increases. This maximum percentage error decreases to 1.5% for $N = 3$, which is the value used to obtain the results presented in this paper.

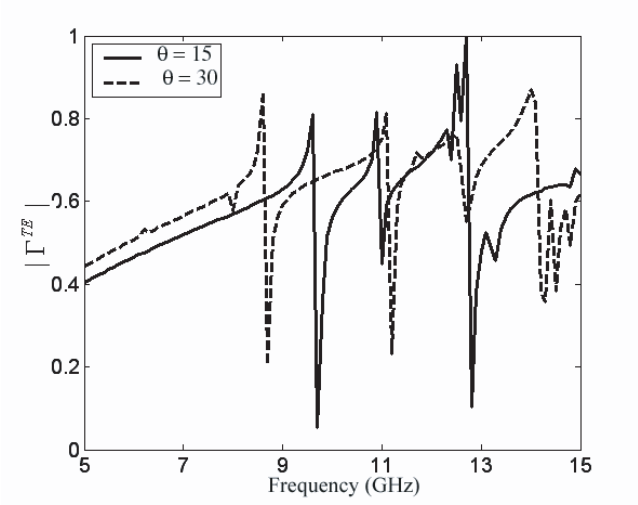

Figure 6. TE reflection coefficients of the same grating structure of Fig. 4. $\phi_{\text{inc}} = 0°$, (a) $\theta_{\text{inc}} = 0°$, (b) $\theta_{\text{inc}} = 15°$ and (c) $\theta_{\text{inc}} = 30°$.

Figure 6 shows the TE reflection of the same grating structures at the same incident angles. It can be noted that due to the symmetry of the embedded dielectric rod with respect to the z-axis, the TE and the TM reflection coefficients are exactly the same at $\theta_{\text{inc}} = 0°$ and $\phi_{\text{inc}} = 0°$, thus it has not been repeated in Fig. 6. By comparing Figures 5 and 6 for different θ_{inc} angles for the same ϕ_{inc} angle it can be noted that the TM resonance frequencies are slightly affected by changing θ_{inc}. However, the number of the TE resonances increases by increasing the elevation angle θ_{inc} and the corresponding resonance frequencies decrease.

Figure 7 shows the dependence of the TE and TM reflection coefficients on the angle ϕ_{inc} for fixed tilting where $\theta_{\text{inc}} = 30°$ for the same grating structure of Figure 4 at 10 GHz. Due to the symmetry of the embedded rod inside the periodic cell, only $\pi/4$ section is sufficient to present the dependence of such reflections coefficients on the angle ϕ_{inc}. Figure 7 shows $\pi/2$ section to show part of this symmetry. It can be noted that, in addition to the frequency selectivity behavior

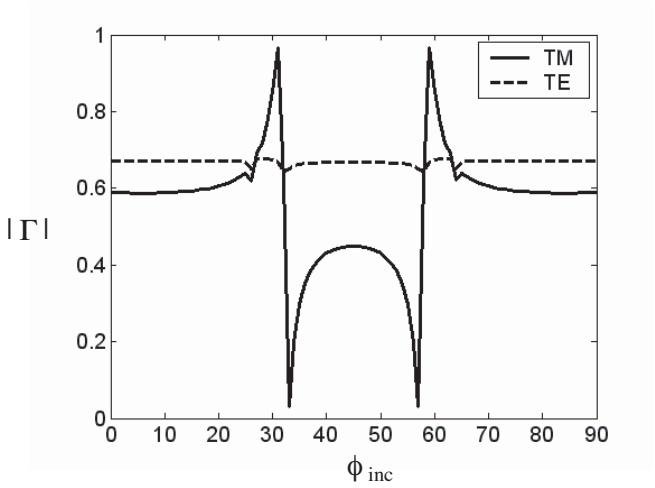

Figure 7. Reflection coefficients at 10 GHz as a function of ϕ_{inc} for the same grating structure of Fig. 4. $\theta_{\text{inc}} = 30^{\circ}$.

of the dielectric grating structure, the angular selectivity can also be obtained for the same frequency as shown in Fig. 7.

It should be noted that all the previous results present only the specular reflection and transmission coefficients. In addition to such specular components, there are also mode conversion components, where the TE incident wave introduces TM wave and vise versa, and non-specular components, which correspond to grating lobes. The existence of these components depends on the dimensions of the periodic cell with respect to the incident wavelength, the coupling effect of the implanted dielectric rods, the direction of incidence and the coupling effect of the embedded rods between the TE and TM waves. Tables 1 and 2 shows samples results for the grating structure of Fig. 4 where it they introduces in addition to its specular wave, other three wave components including coupling between TE and TM waves. The operating frequency in this case is 15 GHz and the direction of incidence is $\theta_{\text{inc}} = 45^{\circ}$ and $\phi_{\text{inc}} = 30^{\circ}$. Power conversion for both TE and TM waves can be easily examined by verifying

$$\sum_{i=1}^{M} \left(\left|\Gamma_i^{TE/TE}\right|^2 + \left|T_i^{TE/TE}\right|^2 + \left|\Gamma_i^{TM/TE}\right|^2 + \left|T_i^{TM/TE}\right|^2 \right) = 1 \quad \text{(22a)}$$

$$\sum_{i=1}^{M} \left(\left|\Gamma_i^{TE/TM}\right|^2 + \left|T_i^{TE/TM}\right|^2 + \left|\Gamma_i^{TM/TM}\right|^2 + \left|T_i^{TM/TM}\right|^2 \right) = 1 \quad \text{(22b)}$$

Table 1. Total reflection coefficients at 15 GHz for the same grating structure of Fig. 4. $\theta_{\text{inc}} = 45°$ and $\phi_{\text{inc}} = 30°$.

Direction of diffracted field	Mode of diffracted field	$\lvert\Gamma^{TE/TE}\rvert$	$\lvert\Gamma^{TM/TE}\rvert$	$\lvert\Gamma^{TE/TM}\rvert$	$\lvert\Gamma^{TM/TM}\rvert$
$\theta = 45°, \phi = 30°$	$(m = 0, n = 0)$	0.558910	0.039539	0.077634	0.467863
$\theta = 27.07°, \phi = -46.55°$	$(m = 0, n = -1)$	0.130430	0.050649	0.097971	0.162806
$\theta = 58.35°, \phi = 137.63°$	$(m = -1, n = 0)$	0.062982	0.063534	0.015651	0.030942
$\theta = 41.08°, \phi = -120.95°$	$(m = -1, n = -1)$	0.131194	0.094718	0.085683	0.128558

Table 2. Total transmission coefficients at 15 GHz for the same grating structure of Fig. 4. $\theta_{\text{inc}} = 45°$ and $\phi_{\text{inc}} = 30°$.

Direction of diffracted field	Mode of diffracted field	$\lvert T^{TE/TE}\rvert$	$\lvert T^{TM/TE}\rvert$	$\lvert T^{TE/TM}\rvert$	$\lvert T^{TM/TM}\rvert$
$\theta = 45°, \phi = 30°$	$(m = 0, n = 0)$	0.756709	0.038788	0.078023	0.881722
$\theta = 27.07°, \phi = -46.55°$	$(m = 0, n = -1)$	0.138850	0.053513	0.070513	0.179749
$\theta = 58.35°, \phi = 137.63°$	$(m = -1, n = 0)$	0.082630	0.064975	0.019104	0.015330
$\theta = 41.08°, \phi = -120.95°$	$(m = -1, n = -1)$	0.131630	0.100221	0.085951	0.141535

where M is the total number of the propagating grating lobes.

Figure 8 shows four-layers 2-D grating slabs as a wide band dielectric FSS. It is composed of four 2-D grating slabs supported by three homogenous dielectric slabs. The unit cell of the 2-D grating slab is a square dielectric ring of $\varepsilon_{rb} = 12$. The dimensions of the unit cell are $D_x = D_y = 10\,\text{mm}$ and the dimensions of the air hole inside the dielectric ring are $L_x = L_y = 7\,\text{mm}$. The thickness of the grating slab is $h_1 = 2\,\text{mm}$. The supporting homogenous dielectric slabs have a dielectric constant $\varepsilon_r = 2.2$ and dielectric thickness $h_2 = 4\,\text{mm}$. Figure 9 shows the transmission and reflection coefficients of this FSS for the case of normally incident plane wave. The results of Fig. 9 are calculated by using both modal analysis and HFSS. The comparison shows good agreement between the two techniques. It can be noted that this FSS structure can be used as a reflecting structure with less than $-20\,\text{dB}$ transmission in the frequency band from 13.2 to 15.6 GHz which is nearly 16.6% bandwidth with respect to its central frequency. It can be also used as a transparent surface for frequencies less than 10 GHz with maximum insertion loss below $-3\,\text{dB}$.

The supporting dielectric slabs have a significant effect on the reflection bandwidth. Figure 10 shows the effect of the dielectric

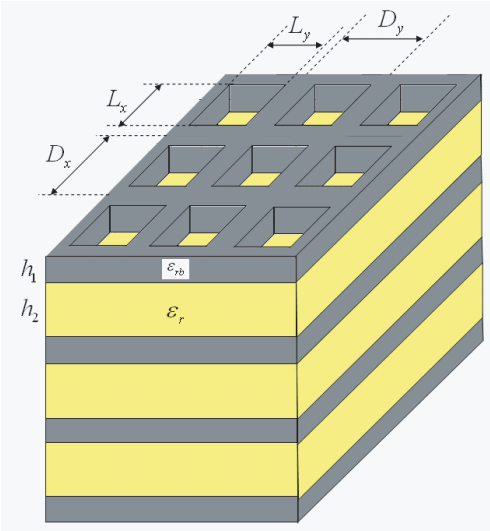

Figure 8. FSS of multilayered dielectric grating slabs. $D_x = D_y = 10\,\text{mm}$, $L_x = L_y = 7\,\text{mm}$, $\varepsilon_{rb} = 12$, $h_1 = 2\,\text{mm}$, $\varepsilon_r = 2.2$ and $h_2 = 4\,\text{mm}$.

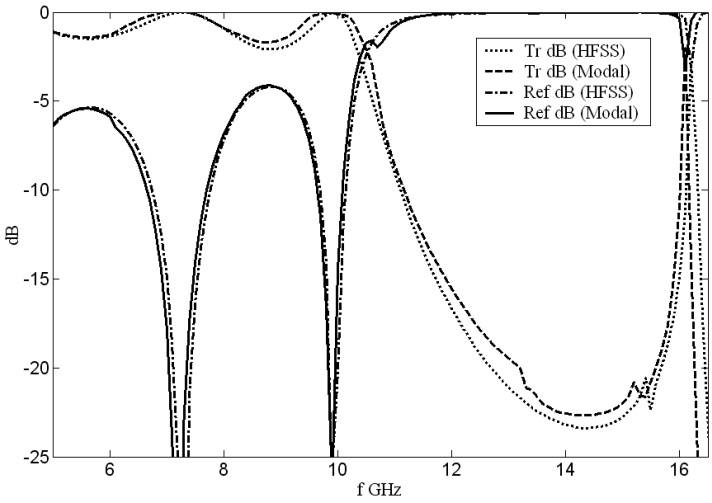

Figure 9. Reflection and Transmission coefficients of multilayered dielectric grating slabs shown in Fig. 8 for the case of normal incidence. $\theta_{\text{inc}} = 0$ and $\phi_{\text{inc}} = 0$. The incident field is y-polarized field.

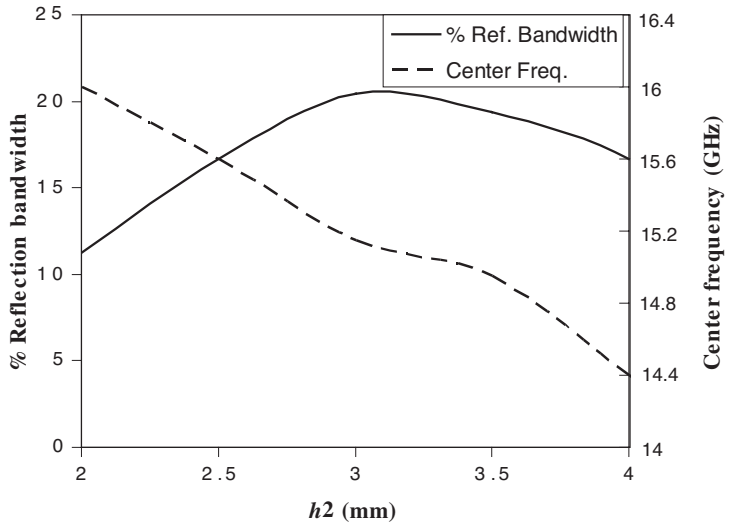

Figure 10. Percentage reflection bandwidth and its corresponding center frequency as functions of supporting slab thickness h_2. The remaining parameters are as shown in Fig. 8.

thickness of the supporting dielectric slab on the reflection bandwidth and the center frequency of the reflection bandwidth where the dielectric constant is ε_r eauals 2.2. It can be noticed that the center frequency of the reflection bandwidth decreases by increasing the thickness of the supporting dielectric slab and the maximum reflection bandwidth for such dielectric constant is nearly 20% at a dielectric thickness h_2 equals 3 mm. Figure 11 shows the effect of the dielectric constant of the supporting dielectric slabs on the reflection bandwidth. It can be noted that the reflection band with increases by decreasing the dielectric constant of the supporting slabs while the center frequency of the reflection bandwidth has slightly decreased

On the other hand, the thickness of the grating structure h_1 has a similar effect on the reflection bandwidth as shown in Figure 12. However the change of the reflection bandwidth is more sensitive to the thickness of the grating structure and the decrease of the center frequency linearly. Finally, Figure 13 shows the effect of base dielectric constant of the grating structure ε_{rb}. It can be noted that the reflection bandwidth increases by increasing ε_{rb} while its center frequency decreases by increasing ε_{rb}.

Based on the above discussions it can be concluded that to design a wideband FSS composed of 2-D dielectric grating slabs of square

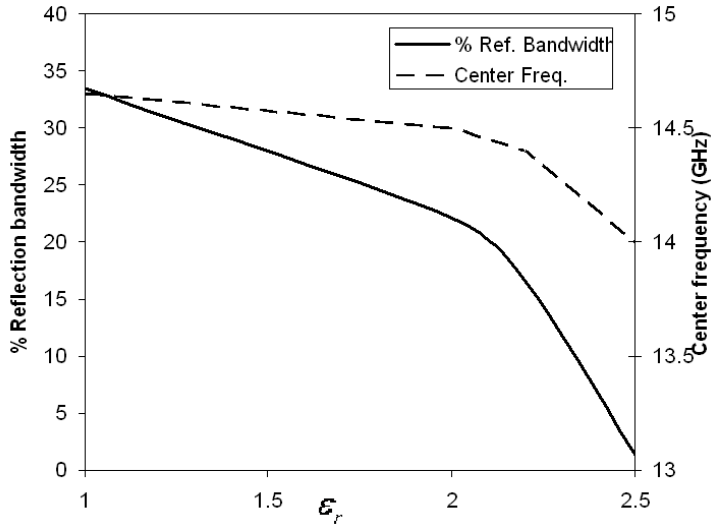

Figure 11. Percentage reflection bandwidth and its corresponding center frequency as functions of supporting slab dielectric constant ε_r. The remaining parameters are as shown in Fig. 8.

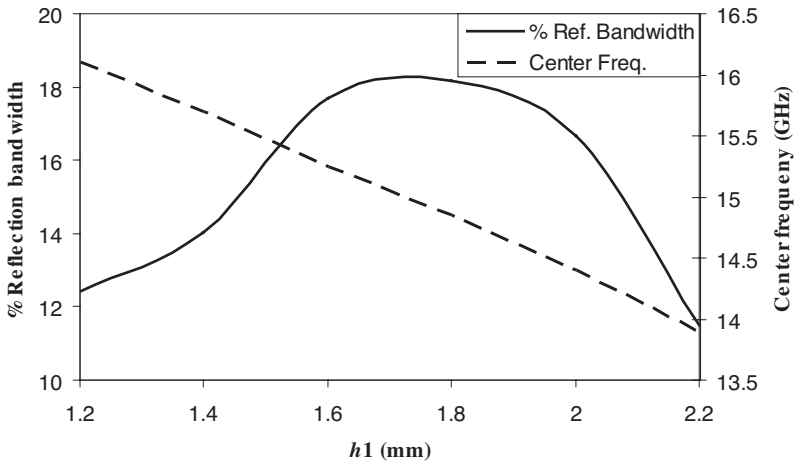

Figure 12. Percentage reflection bandwidth and its corresponding center frequency as functions of grating slab thickness h_1. The remaining parameters are as shown in Fig. 8.

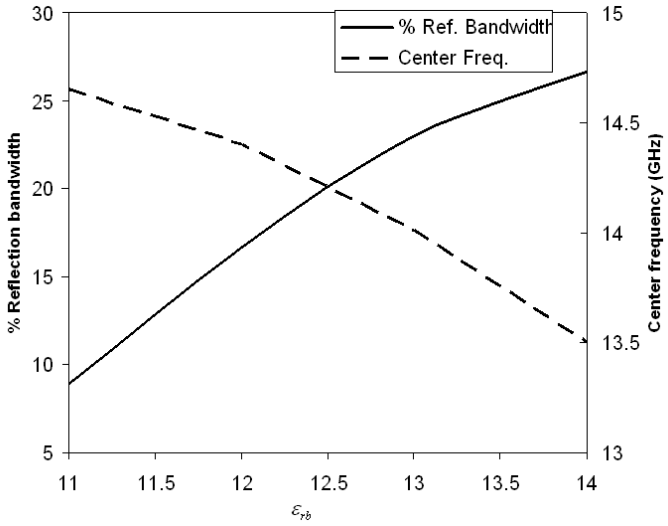

Figure 13. Percentage reflection bandwidth and its corresponding center frequency as functions of ε_{rb}. The remaining parameters are as shown in Fig. 8.

dielectric rings supported by homogenous dielectric slabs it is required to increase the base dielectric constant of the grating structure and to decrease the dielectric constant of the supporting dielectric slab. The thicknesses of the grating slab and the support slabs have significant effects on the reflection bandwidth. Appropriate choice of these thicknesses is required to obtain maximum reflection bandwidth.

5. CONCLUSION

An efficient approach to study the reflection and transmission coefficients of two-dimensional dielectric grating structures for arbitrary incident plane wave was presented. The approach was based on vectorial modal analysis of the grating structure to obtain the field distribution and the propagation constant of different modes in the grating structure. The modal analysis was combined with the generalized scattering matrix. The reflection and transmission coefficients of multilayered two-dimensional dielectric grating structure were obtained. The technique was verified by comparing the results of the present approach with previously published results based on experimental and other numerical techniques. The present modal analysis required expanding the field in the transverse direction

only while the method of moments based on volume integral equation requires expanding the field in the three-dimensional space, which requires more expansion functions especially for thick grating structures. A wideband FSS composed of multilayered grating slabs supported by homogeneous dielectric slabs was designed. It was also found that this approach requires less Floquet modes for convergence as compared with the Method of Moment.

REFERENCES

1. Coves, A., B. Gimeno, J. Gil, M. V. Andres, A. A. San Blas, and V. E. Boria, "Full-wave analysis of dielectric frequency-selective surfaces using vectorial modal method," *IEEE Trans. Antennas Propagat.,* Vol. 52, 2091–2099, Aug. 2004.
2. Coves, A., B. Gimeno, A. A. San Blas, A. Vidal, V. E. Boria, and M. V. Andres, "Three-dimensional scattering of dielectric gratings under plane-wave excitation," *IEEE Antennas and Wireless Propagation Letters,* Vol. 2, 215–218, 2003.
3. Peng, S. T., T. Tamir, and H. L. Bertoni, "Theory of periodic dielectric waveguides," *IEEE Trans. Microwave Theory Techniques,* Vol. 23, 123–133, Jan. 1975.
4. Peng, S. T., "Rigorous formulation of scattering and guidance by dielectric grating waveguides: General case of oblique incidence," *J. Opt. Soc. Amer. A.,* Vol. 6, No. 12, 1869–1883, Dec. 1989.
5. Bertoni, H. L., L. H. S. Cheo, and T. Tamir, "Frequency-selective reflection and transmission by a periodic dielectric layer," *IEEE Trans. Antennas Propagat.,* Vol. 37, 78–83, Jan. 1989.
6. Pai, D. M. and K. A. Awada, "Analysis of dielectric gratings of arbitrary profiles and thicknesses," *J. Opt. Soc. Amer. A.,* Vol. 8, No. 5, 755–762, May 1991.
7. Yang, H. Y. D., R. Diaz, and N. G. Alexopoulos, "Reflection and transmission of waves from multilayer structures with planar-implanted periodic material blocks," *J. Opt. Soc. Amer. B.,* Vol. 14, 2513–2521, Oct. 1997.
8. Tibuleac, S., R. Magnusson, T. A. Maldonado, P. P. Young, and T. R. Holzheimer, "Dielectric frequency-selective structures incorporating waveguide gratings," *IEEE Trans. Microwave Theory Tech.,* Vol. 48, 553–561, Apr. 2000.
9. Mosallaei, H. and Y. Rahmat-Samii, "Periodic bandgap and effective dielectric materials in electromagnetics: characterization and applications in nanocavities and waveguides," *IEEE Trans. Antennas Propagat.,* Vol. 51, 549–563, Mar. 2003.

10. Costa, J. C. W. A. and A. J. Giarola, "Electromagnetic wave propagation in multilayer dielectric periodic structures," *IEEE Trans. Antennas Propagat.,* Vol. 41, 1432–1438, Oct. 1993.
11. Jarem, J. M. and P. P. Banerjee, *Computational Methods for Electromagnetic and Optical Systems,* Marcel Dekker, Inc., 2000.
12. Moharam, M. G., E. B. Grann, D. A. Pommet, and T. K. Gaylord, "Formulation for stable and efficient implementation of the rigorous coupled-wave analysis of binary grating," *J. Opt. Soc. Am. A.,* Vol. 12, 1068–1076, May 1995.
13. Silvestre, E., M. A. Abian, B. Gimeno, A. Ferrando, M. V. Andres, and V. E. Boria, "Analysis of inhomogeneously filled waveguides using a bi-orthonormal-basis method," *IEEE Trans. Microwave Theory Tech.,* Vol. 48, 589–596, Apr. 2000.
14. Mittra, R., C. H. Chan, and T. Cwik, "Techniques for analyzing frequency selective surfacesa review," *Proc. IEEE,* Vol. 76, 1593–1615, Dec. 1988.